2004

Photonic Band Gap Analysis Using Finite-Difference Frequency-Domain Method

Shangping Guo
Old Dominion University

Feng Wu
Old Dominion University

Sacharia Albin

Original Publication Citation

Guo, S., Wu, F., Albin, S., & Rogowski, R. S. (2004). Photonic band gap analysis using finite-difference frequency-domain method. *Optics Express, 12*(8), 1741-1746. doi:10.1364/OPEX.12.001741

Photonic band gap analysis using finite-difference frequency-domain method

Shangping Guo, Feng Wu, Sacharia Albin

Photonics Laboratory, Department of Electrical & Computer Engineering
Old Dominion University, Norfolk, Virginia 23529
sguo@odu.edu

Robert S. Rogowski

Non-destructive Evaluation Science Branch, NASA Langley Research Center, Hampton, Virginia 23681

Abstract: A finite-difference frequency-domain (FDFD) method is applied for photonic band gap calculations. The Maxwell's equations under generalized coordinates are solved for both orthogonal and non-orthogonal lattice geometries. Complete and accurate band gap information is obtained by using this FDFD approach. Numerical results for 2D TE/TM modes in square and triangular lattices are in excellent agreements with results from plane wave method (PWM). The accuracy, convergence and computation time of this method are also discussed.

OCIS code: (350.3950) Micro-optics (260.2110) Electromagnetic theory

References and links

1. E. Yablonovitch, "Inhibited Spontaneous Emission in Solid-State Physics and Electronics," Phys. Rev. Lett. **58**, 2059-2062 (1987).
2. S. John, "Strong localization of photons in certain disordered dielectric superlattices," Phys. Rev. Lett. **58**, 2486-2489 (1987).
3. K. M. Ho, C. T. Chan, and C. M. Soukoulis, "Existence of a photonic gap in periodic dielectric structures," Phys. Rev. Lett. **65,** 3152-3155 (1990).
4. R. D. Meade, A. M. Rappe et al., "Accurate theoretical analysis of photonic band gap materials," Phys. Rev. B **48,** 8434-8437 (1993).
5. K. M. Leung and Y. F. Liu, "Full vector wave calculation of photonic band structures in FCC dielectric media," Phys. Rev. Lett. **65,** 2646-2649 (1990).
6. M. Qiu, S. He, "A nonorthogonal finite-difference time-domain method for computing the band structure of a two-dimensional photonic crystal with dielectric and metallic inclusions ," J. Appl. Phys. **87**, 8268-8275 (2000).
7. C. T Chan, Y. L. Yu, K. M. Ho, "Order-N spectral method for electromagnetic waves," Phys. Rev. B **51**, 16635-16642 (1995).
8. J. Arriaga, A. J. Ward and J. B. Pendry, "Order-*N* photonic band structures for metals and other dispersive materials," Phys. Rev. B **59**, 1874-1877 (1999).
9. A. J. Ward and J. B. Pendry, "Refraction and geometry in Maxwell's equations," J. Mod. Opt. **43**, 773-793 (1996).
10. Z. Zhu, T. G. Brown, "Full vectorial finite difference analysis of microstructured optical fibers," Opt. Express **10**, 853-864 (2002). http://www.opticsexpress.org/abstract.cfm?URI=OPEX-10-17-853
11. K. Bierwith, N. Schulz, F. Arndt, "Finite-difference analysis of rectangular dielectric waveguide structures," IEEE Trans. Microwave Theory Tech. **34**, 1104-1113 (1986).
12. P. Lusse, P. Stuwe, J Schule, H. G. Unger, "Analysis of vectorial mode fields in optical waveguides by a new finite-difference method," J. Lightwave Technol. **12**, 487-494 (1994).
13. H Y D Yang, "Finite-difference analysis of 2D photonic crystals," IEEE Trans. Microwave Theory Tech. **44,** 2688-2695 (1996).
14. K.S Yee, "Numerical solution of initial boundary value problems involving Maxwell's equations in isotropic media," IEEE Trans. Antennas Propagat. **14**, 302-307 (1966).
15. A. J. Ward, "Order-N program documentation," http://www.sst.ph.ic.ac.uk/photonics/ONYX/orderN.html
16. S. Guo, S. Albin, "Simple plane wave implementation for photonic crystal calculations," Opt. Express **11**, 167-175 (2003). http://www.opticsexpress.org/abstract.cfm?URI=OPEX-11-2-167
17. S. Guo, S. Albin, "Numerical techniques for excitation and analysisof defect modes in photonic crystals," Opt. Express **11**, 1080-1089 (2003). http://www.opticsexpress.org/abstract.cfm?URI=OPEX-11-9-1080

#4061 - $15.00 US Received 22 March 2004; revised 7 April 2004; accepted 7 April 2004

18. P R McIssac, "Symmetry induced modal characteristics of uniform waveguides-I: Summary of results," IEEE Trans. MTT **23**, 421-429 (1975).

1. Introduction

Photonic band gap materials and devices have been under intense research for over a decade following the seminal papers [1-2]. There are several methods for band structure analysis, such as the plane wave method (PWM) [3-5] and the FDTD [6-9] method. The PWM is able to provide complete and accurate information. However, the algorithm complexity is $O(N^3)$ and the computation is heavy for large problems. The order-N method based on FDTD can effectively reduce computation. It solves the Maxwell's equations within the unit cell in time-domain by applying an initial field that covers all the possible symmetries; the eigen-modes are identified as the spectral peaks from the Fourier transform of the time-variant fields. The drawback of this method is that the accuracy depends on the number of iterations in time. There is also a possibility of losing true eigen-mode if the corresponding peak is too small, or resolution is too low. Moreover, spurious modes may arise from spectral noise. The FDFD method has been proposed for optical waveguide analysis [10-12], which is accurate and stable. In this paper, we show that this technique can be applied in photonic band gap analysis and we note that an FDFD approach using Helmholtz equation has been shown in [13]. First we describe the derivation of the FDFD algorithm under generalized coordinate system and then apply the algorithm on 2D photonic crystals with two different geometries. The accuracy, convergence, and computation time in the FDFD method are compared with those of PWM.

2. Theory

We consider nonconductive materials under generalized coordinates denoted by three unit basis vectors $u_q(x,y,z)$ (q=1,2,3). The Maxwell's curl equations in complex form can be expressed as [9, 15]:

$$\nabla_q \times \hat{H} = jk_0 \hat{\varepsilon}(r)\hat{E} \qquad \nabla_q \times \hat{E} = -jk_0 \hat{\mu}(r)\hat{H}\,, \tag{1}$$

and the renormalized fields are: $\hat{E}_i = Q_i \sqrt{\varepsilon_0/\mu_0}\, E_i \quad \hat{H}_i = Q_i H_i\,,$ (2)

where k_0 is the wave vector in free space, Q_i's are the grid size along each direction. The $\hat{\varepsilon}$ and $\hat{\mu}$ are respectively the effective relative permitivity and permeability constants which are 3x3 tensors under the generalized coordinate system:

$$\hat{\varepsilon}_{ij}(r) = \varepsilon_{ri}(r) g_{ij} \left|u_1 \cdot u_2 \times u_3\right| \frac{Q_1 Q_2 Q_3}{Q_i Q_j Q_0} \quad \hat{\mu}_{ij}(r) = \mu_{ri}(r) g_{ij} \left|u_1 \cdot u_2 \times u_3\right| \frac{Q_1 Q_2 Q_3}{Q_i Q_j Q_0}\,. \tag{3}$$

Q_0 is a constant introduced to be roughly equal to Q_i's; $\left|u_1 \cdot u_2 \times u_3\right|$ is the volume of the unit cell, ε_{ri} (μ_{ri}) is the relative dielectric constant (the relative permeability constant) at the position where the electric field $\hat{E}_i$ (the magnetic field $\hat{H}_i$) is located. $\boldsymbol{g}$ is the metric tensor that can be obtained using the three unit vectors,

$$g^{-1} = \begin{bmatrix} u_1 \cdot u_1 & u_1 \cdot u_2 & u_1 \cdot u_3 \\ u_2 \cdot u_1 & u_2 \cdot u_2 & u_2 \cdot u_3 \\ u_3 \cdot u_1 & u_3 \cdot u_2 & u_3 \cdot u_3 \end{bmatrix} \tag{4}$$

and the length in generalized coordinate can be calculated using:

$$\left|r^2\right| = \vec{r}^{\,T} \left[g^{-1}\right] \vec{r}\,. \tag{5}$$

#4061 - $15.00 US Received 22 March 2004; revised 7 April 2004; accepted 7 April 2004

We use Yee's mesh [14] and finite difference to replace the derivates in Maxwell's curl equations [9, 15] and formulate them in matrix form using the approach described in [10]:

$$jk_0\begin{bmatrix}\hat{E}_1\\ \hat{E}_2\\ \hat{E}_3\end{bmatrix}=\begin{bmatrix}\varepsilon_{11}^{-1} & \varepsilon_{12}^{-1} & \varepsilon_{13}^{-1}\\ \varepsilon_{21}^{-1} & \varepsilon_{22}^{-1} & \varepsilon_{23}^{-1}\\ \varepsilon_{31}^{-1} & \varepsilon_{32}^{-1} & \varepsilon_{33}^{-1}\end{bmatrix}\begin{bmatrix}0 & -U_3 & U_2\\ U_3 & 0 & -U_1\\ -U_2 & U_1 & 0\end{bmatrix}\begin{bmatrix}\hat{H}_1\\ \hat{H}_2\\ \hat{H}_3\end{bmatrix}, \tag{6}$$

$$-jk_0\begin{bmatrix}\hat{H}_1\\ \hat{H}_2\\ \hat{H}_3\end{bmatrix}=\begin{bmatrix}\mu_{11}^{-1} & \mu_{12}^{-1} & \mu_{13}^{-1}\\ \mu_{21}^{-1} & \mu_{22}^{-1} & \mu_{23}^{-1}\\ \mu_{31}^{-1} & \mu_{32}^{-1} & \mu_{33}^{-1}\end{bmatrix}\begin{bmatrix}0 & -V_3 & V_2\\ V_3 & 0 & -V_1\\ -V_2 & V_1 & 0\end{bmatrix}\begin{bmatrix}\hat{E}_1\\ \hat{E}_2\\ \hat{E}_3\end{bmatrix}, \tag{7}$$

where U_i and V_i are coefficient matrices formed according to the boundary conditions, and they are proportional to $1/Q_i$.

An eigen-value problem in frequency-domain is formed for either $\hat{E}$ or $\hat{H}$ by eliminating $\hat{H}$ or $\hat{E}$ in Eqs. (6-7). For a given wave vector k, all the referred components outside the unit cell boundary can be obtained using Bloch's periodic boundary condition:

$$\hat{H}(r+R_l)=\exp(ik\cdot R_l)\hat{H}(r)\quad \hat{E}(r+R_l)=\exp(ik\cdot R_l)\hat{E}(r), \tag{8}$$

where R_l can be an arbitrary lattice vector, and here it is limited in the unit cell or supercell.

Two-dimensional cases

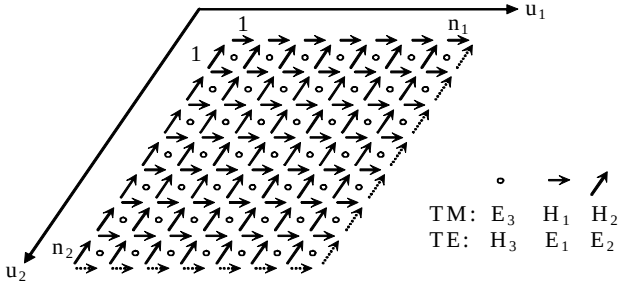

Fig. 1. Yee's 2D mesh in general coordinates. The dotted components are at the boundaries.

A 2D Yee's mesh under generalized coordinate system is shown in Fig. 1 for both TE and TM modes. E and H are arranged along two basis vectors u_1 and u_2; u_3 is coincident with the z direction. Since Q_3 is infinite, U_3 and V_3 in the equation (6-7) are zero, and simple eigen-equations can be obtained. The lattice vector R_l in Eq. (8) is chosen to be $a_q u_q$, and a_q is the dimension of the unit cell or supercell along direction *q*.

For TM modes, the eigen-equation is shown as follows:

$$k_0^2\hat{E}_z=\varepsilon_{33}^{-1}\left\{U_1\left(\mu_{21}^{-1}V_2-\mu_{22}^{-1}V_1\right)-U_2\left(\mu_{11}^{-1}V_2-\mu_{12}^{-1}V_1\right)\right\}\hat{E}_z. \tag{9}$$

The fields E and H in the two dimensional grids are arranged row by row into column vectors. Subsequently the Bloch boundary conditions are applied to get the matrices U and V:

#4061 - $15.00 US Received 22 March 2004; revised 7 April 2004; accepted 7 April 2004

$$U_1 = \frac{1}{Q_1}\begin{bmatrix} -1 & 1 & & & & & & \\ & \ddots & \ddots & & & & & \\ u_x & & -1 & 0 & & & & \\ & & & \ddots & \ddots & & & \\ & & u_x & & -1 & 0 & & \\ & & & & & -1 & \ddots & \\ & & & & u_x & & \ddots & 1 \\ & & & & & & & -1 \end{bmatrix}, \quad V_1 = \frac{1}{Q_1}\begin{bmatrix} 1 & & v_x & & & & & \\ -1 & \ddots & & & & & & \\ & \ddots & 1 & & & & & \\ & & 0 & \ddots & & v_x & & \\ & & & \ddots & 1 & & & \\ & & & & 0 & 1 & & v_x \\ & & & & & \ddots & \ddots & \\ & & & & & & -1 & 1 \end{bmatrix} \tag{10}$$

where
$$u_x = \exp(ik \cdot a_1 u_1), \; v_x = -\exp(-ik \cdot a_1 u_1) \tag{11}$$

$$U_2 = \frac{1}{Q_2}\begin{bmatrix} -1 & & 1 & & & \\ & -1 & & 1 & & \\ & & \ddots & & \ddots & \\ & & & \ddots & & \ddots \\ & & & & -1 & \\ u_y & & & & & 1 \\ & \ddots & & & -1 & \\ & & u_y & & & -1 \end{bmatrix}, \quad V_2 = \frac{1}{Q_2}\begin{bmatrix} 1 & & -1 & & & \\ & 1 & & -1 & & \\ & & \ddots & & \ddots & \\ & & & \ddots & & \ddots \\ & & & & 1 & \\ v_y & & & & & -1 \\ & \ddots & & & 1 & \\ & & v_y & & & 1 \end{bmatrix} \tag{12}$$

where
$$u_y = \exp(ik \cdot a_2 u_2), \; v_y = -\exp(-ik \cdot a_2 u_2). \tag{13}$$

For TE modes, the eigen-equation is:

$$k_0^2 \hat{H}_z = \left\{ \varepsilon_{12}^{-1} U_1 \mu_{33}^{-1} V_2 - \varepsilon_{22}^{-1} U_1 \mu_{33}^{-1} V_1 \right\} \hat{H}_z . \tag{14}$$

The U and V matrices for TE mode are similar to those for TM modes and can be obtained by doing the exchange $U_1 \Leftrightarrow V_1$ and $U_2 \Leftrightarrow V_2$ in the equations (10-13) for TM modes.

According to Eq. (9), only ε_{33}^{-1} is involved in TM mode. ε_r is located at the same point as E_3, so no averaging is needed for ε_{r3}. For TE mode, the ε_r is half a grid away from E_1 and E_2 and the averaging is needed for ε_{r1} and ε_{r2}. The periodicity of ε_r is applied for those grids outside the boundary.

3. Numerical results

All matrices involved are sparse; hence we can apply sparse matrix techniques to save computation time and memory. We implemented the algorithm using MATLAB since it provides convenient tools for sparse matrix operation with minimal programming efforts. Here we show a few numerical examples using our FDFD method and compare against the PWM using the program similar to that in Ref. [16]. The first example is a 2D square lattice with dielectric alumina rods in air: ε_a=8.9, ε_b=1.0 and radius of the rod R=0.20*a* (*a* is the lattice constant). The second example is a 2D triangular lattice with air holes in dielectric GaAs materials: ε_a=1.0, ε_b=13.0 and hole radius R=0.20*a*. For the square lattice u_1=[1 0 0], u_2=[0 1 0], and u_3=[0 0 1] and the metric [g] is a 3x3 identity matrix. For the triangular lattice, u_1=[1 0 0], u_2=[0 1/2 $\sqrt{3}/2$], and u_3=[0 0 1] and [g] is calculated by Eq. (4). We used sub-cell averaging technique to smooth the transition at the interface and Eq. (5) is used for the rod profile transformation. The details of discretization and transformation of the cylindrical rod are shown in Ref. [16].

#4061 - $15.00 US
Received 22 March 2004; revised 7 April 2004; accepted 7 April 2004

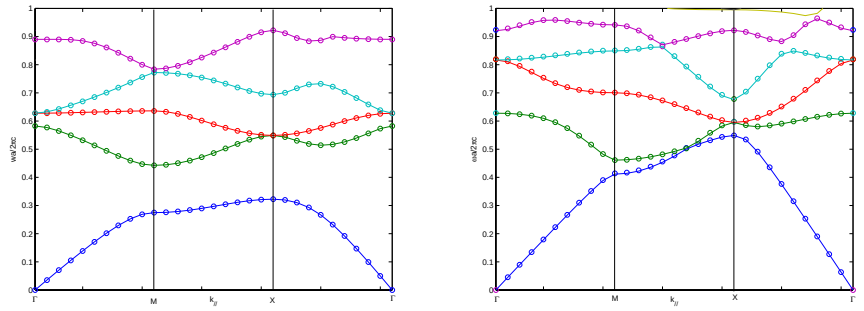

Fig. 2. The band structure for a 2D square lattice by FDFD (o) and PWM (-). 441 plane waves are used for PWM and mesh resolution is a/80 for FDFD. Left: TM mode, Right: TE mode.

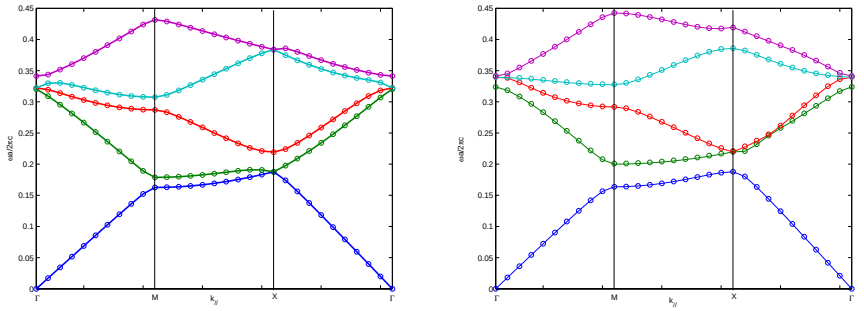

Fig. 3. The calculated band structure of a triangular lattice by FDFD (o) and PWM (-). 441 plane waves are used for PWM and mesh resolution is a/80 for FDFD. Left: TM, Right: TE.

The TE/TM band gap for 2D square lattice and triangular lattice of the above examples are shown in Fig. 2 and Fig. 3 respectively. The FDFD results are indicated by 'o' and PWM results are plotted as solid lines. The results from the two methods show excellent agreements.

In Table 1 we list the first five bands at k=0 for the 2D triangular lattice shown above using the two methods in order to compare their accuracy and computation time. The computation time is measured on a 2.4GHz mobile Celeron® notebook with 256MB memory. From the Table we see that FDFD can reach the same accuracy as PWM in a shorter time.

Table 1. Eigen-frequencies for the first five bands of TE wave (k=0) for a triangular lattice with air holes in dielectric materials.

Band No:	1	2	3	4	5	Time (s)
PWM 441[1]	0	0.3240	0.3398	0.3399	0.3414	47.84
PWM 625[1]	0	0.3240	0.3399	0.3399	0.3414	105.66
PWM 961[1]	0	0.3240	0.3400	0.3400	0.3414	256.36
FDFD 40[2]	0	0.3237	0.3395	0.3400	0.3418	3.29
FDFD 80[2]	0	0.3240	0.3400	0.3402	0.3416	11.68
FDFD 120[2]	0	0.3240	0.3400	0.3402	0.3415	33.18
FDFD 160[2]	0	0.3240	0.3401	0.3402	0.3414	86.09

1: The number of plane waves, 2: the number of grids along each direction.

A convergence curve for the eigen-frequency of band 5 at k=0 is shown in Fig. 4 versus the number of grids used along each direction. The computation time is also presented in the figure. The eigen-values converge to the accurate value at a moderate mesh size, for example, a/80. The computation time is highly dependent on the memory available on the computer.

#4061 - $15.00 US Received 22 March 2004; revised 7 April 2004; accepted 7 April 2004

When the unit cell or supercell has symmetry properties, computation time could be saved by using part of the unit cell under proper boundary conditions [18].

Next, we show a defect mode analysis using FDFD for the 2D square lattice of alumina rods in air as in the first example. A 5x5 supercell is selected and 200 grids are used along each direction. In this case, only the defect frequency is of interest since the band gap information is already known. Therefore we only have to find a certain number of eigen-frequencies of interest and the computation time is effectively reduced. The eigen-frequency obtained by FDFD is 0.3930. The mode field is shown in Fig. 5. Both results agree well with those by PWM and FDTD [16-17].

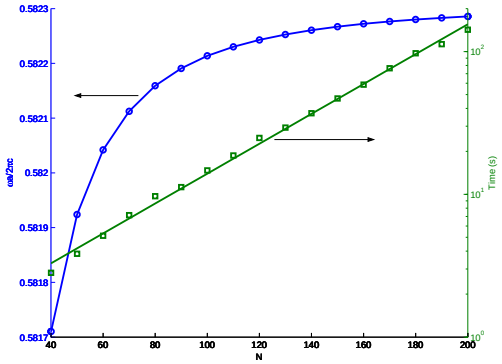

Fig. 4. The convergence of eigen-frequency (the 5th band at k=0) and the computation time vs. the number of grids along each direction.

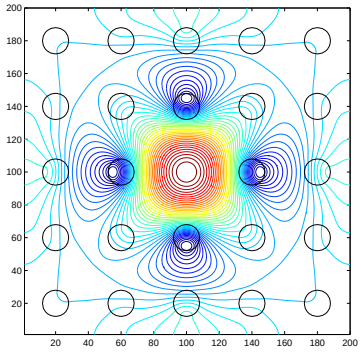

Fig. 5. The E_z field of a defect mode in a 2D square lattice with alumina rods in air using a 5x5 supercell with the center rod removed. The rods are displayed as black circles.

4. Conclusions

In conclusion, we have presented a FDFD method for photonic band gap calculations. This method is able to provide complete and accurate information about the band structure of a photonic crystal. The results of 2D TE/TM modes for two different geometries are compared with those obtained using plane wave method, and excellent agreement is achieved. By using a generalized coordinate system, various lattice geometries can be analyzed in the same manner.

Acknowledgments

The research at Old Dominion University is supported by NASA Langley Research Center through NASA-University Photonics Education and Research Consortium (NUPERC). We thank the reviewer for bringing references [11-13] to our attention.

#4061 - $15.00 US Received 22 March 2004; revised 7 April 2004; accepted 7 April 2004